A DIRECTIONAL IMAGE DECOMPOSITION FOR ULTRA-WIDEBAND SAR

Richard Rau and James H. McClellan

Center for Signal and Image Processing
School of Electrical and Computer Engineering
Georgia Institute of Technology
Atlanta, Georgia, USA
richard@ece.gatech.edu

ABSTRACT

This paper presents a theoretical analysis of the structure of wide angle, ultra-wideband SAR images formed by a constant integration angle backprojection image former. It is shown that the effects of the image former can be modeled as a filtering operation on the original data. Furthermore, SAR images for different squint angles can be obtained from the original images by directional filtering. As a result, it will be shown that perfect reconstructing directional filterbanks can be used as a unitary transform between SAR images and a 3-D representation containing additional aspect-angle information. It will be demonstrated, how this new representation can be used to enhance targets.

1. INTRODUCTION

Low-frequency, wide angle, ultra-wideband (UWB) SARs provide high downrange and crossrange resolution and can penetrate foliage and soil to detect obscured targets. Recent research [3, 7] has focused on extracting additional target information to improve the discrimination of natural and man-made targets. A commonly exploited difference between man-made and natural targets is the aspect angle dependence of their respective responses. Extended flat objects, which can roughly be approximated by a dihedral, exhibit a very pronounced sideflash, i.e. a large response over a very small range of aspect angles and a small response for all other aspect angles. On the other hand, cylindrical objects such as tree trunks have responses with very little aspect angle dependence. This basic difference cannot be exploited by traditional SARs, which image targets only over a few degrees aspect angle. Wide angle SARs, on the other hand, can span aspect angle ranges of 90° and more. Up to now the processing needed to extract angle information was mostly done before the image formation. Since several SAR images often have to be computed, this approach is computationally very expensive.

We will demonstrate here that the same information can be obtained from SAR images by an adequately designed post-processing step. Furthermore, we will show that directional filterbanks can be used to generate an alternative 3-D representation of SAR images, which simplifies extracting aspect angle properties of targets.

This work was prepared through collaborative participation in the Advanced Sensors Consortium sponsored by the U.S. Army Research Laboratories under cooperative agreement DAAL01-96-2-0001.

It was also supported by the Joint Services Electronics Program under contract DAAH-04-96-1-0161.

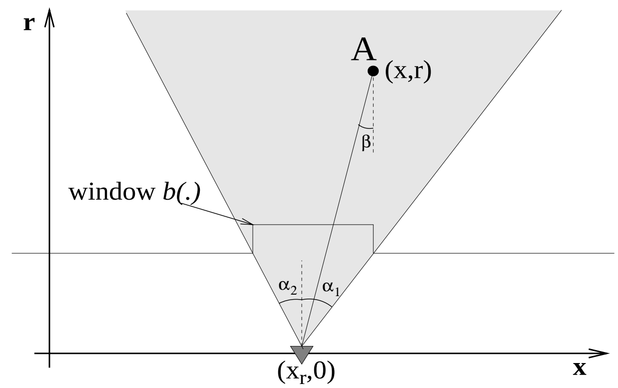

Figure 1: Data collection geometry for strip map SAR.

The paper is structured as follows. First we outline briefly the strip map SAR geometry. In section 3 we define and analyze a four parameter reflectivity model and derive the Fourier transform of the raw data received by the radar. Section 4 provides a closed form expression for the Fourier transform of SAR images generated with a constant integration angle image former. It will be shown in section 5 that images formed from subapertures can be obtained by directionally filtering the SAR images. A very brief introduction to directional filterbanks follows and it will be shown that the subbands of a directional filterbank are equivalent to SAR images formed from subapertures. An example of the new 3-D data representation is given in section 6. Finally, in section 7, we demonstrate how a directional filterbank can be used to enhance man-made targets.

2. STRIP MAP SAR

Figure 1 shows the data collection geometry of a strip map SAR. We consider here only the 2-D case with the radar and the illuminated area in one plane. The radar is moved along the x-axis. At regular intervals the antenna emits a pulse and records all returns reflected by the targets within the radar beam as a one-dimensional time signal $d(x_r, t)$, where x_r is the radar location. Small displacements of the radar between transmitting and receiving due to the continuous motion of the radar platform are normally negligible and will be omitted here. The radar beam is shown in gray. Its width and squint can be specified by the two angles α_1 and α_2 or alternatively by a window $b(\frac{x_r - x}{r})$. Characterizing the beam by $b(\cdot)$ has the advantage that intensity profile information about the beam can be incorporated into the shape of $b(\cdot)$. Point A in Fig. 1 denotes an arbitrary reflector. The transmitted wave reaches point A under the aspect angle β. It can easily be seen that β varies over the interval $[\alpha_1, \alpha_2]$ while the radar passes point A. The set of all radar locations when receiving data is the radar aperture. Although the aperture is inherently discrete, we use a continuous aperture for our derivations and consider quantization of the derived results later.

3. RAW DATA MODEL

Frequently the illuminated area in SAR imaging is modeled as a two-dimensional reflectivity profile $g(x, r)$, which depends on crossrange (x) and down-range (r)position. This simple model is, however, not appropriate for wide angle, ultra-wideband SARs. The high bandwidth of the transmitted pulses requires taking into account the frequency dependence of the target reflectivity. The large beamwidth $[\alpha_2, \alpha_1]$ leads to target illumination over a large range of aspect angles β. However, the reflectivity profile will change with the aspect angle due to occlusions and angular variations of target reflectivities. Thus, a more elaborate signal model is necessary.

We incorporate both frequency and aspect angle dependence of targets into $g(x, r)$ by adding two additional degrees of freedom:

$$g(x, r, t, \tan\beta) \quad \text{with} \quad \beta \in [-\frac{\pi}{2}, \frac{\pi}{2}] \tag{1}$$

If the radar is at location x_r, then $\tan\beta$ with respect to x_r and a point (x, r) is given as:

$$\tan\beta = \frac{x_r - x}{r} \tag{2}$$

The same reflectivity model extensions were proposed in [1]. Let $p(t)$ be the transmitted waveform of the radar. Then the received signal $d(x, t)$ has the following form:

$$\begin{aligned} d(x,t) \quad = \quad & \int\int \frac{1}{\sqrt{\hat{r}}} b\left(\frac{x-\hat{x}}{\hat{r}}\right) g\left(\hat{x}, \hat{r}, t, \frac{x-\hat{x}}{\hat{r}}\right) *_t \\ & p(t) *_t \delta\left(t - \frac{2}{c}\sqrt{(x-\hat{x})^2 + \hat{r}^2}\right) d\hat{x}d\hat{r} \end{aligned} \tag{3}$$

where $*_t$ denotes convolution with respect to time and $\delta(t)$ a Dirac impulse. The term $\frac{1}{\sqrt{r}}$ normalizes the energy of the window $b(\cdot)$ to a r independent constant. The Fourier transform of (3) reveals more details about the structure of the data. While it is straightforward to compute the Fourier transform of (3) with respect to t, it is quite involved to compute the Fourier transform with respect to x. We have to solve an integral of the general form:

$$\int f(x) e^{j(k_x x - \omega \frac{2}{c}\sqrt{x^2+r^2})} dx \tag{4}$$

This integral cannot be written in closed form. However, the principle of stationary phase [2, 10] can be applied, which establishes the following approximation for a class of integrals [10]:

$$\int f(t) e^{-jxp(t)} dt \approx f(\tau)\sqrt{\frac{2\pi}{jxp''(\tau)}} e^{-jxp(\tau)} \quad \text{for} \quad x \to \infty \tag{5}$$

The instant τ is given as the root of the first derivative of $p(t)$.

If we apply (5) to our problem, we can solve not only the Fourier integral but also the two integrals with respect to $\hat{x}$ and $\hat{r}$. We obtain the following approximation:

$$D(k_x, \omega) = \begin{cases} AP(\omega) b\left(\frac{k_x \text{sgn}(\omega)}{\mu(\omega, k_x)}\right) * \\ \quad g^{x,r,t}\left(k_x, -\text{sgn}(\omega)\mu(\omega, k_x), \omega, \frac{k_x \text{sgn}(\omega)}{\mu(\omega,k_x)}\right) * \\ \quad |\omega| \mu(\omega, k_x)^{-1.5} e^{-j\text{sgn}(\omega)\frac{\pi}{4}} & \text{for } |k_x| < |2\frac{\omega}{c}| \\ \approx 0 & \text{otherwise} \end{cases} \tag{6}$$

with

$$\mu(\omega, k_x) = \sqrt{(2\frac{\omega}{c})^2 - k_x^2} \tag{7}$$

The function $g^{x,r,t}(\cdot,\cdot,\cdot,\cdot)$ is the 3-D Fourier transform of (1) with respect to its first three parameters. A is used here and in the following derivations as a context dependent constant.

4. ANALYSIS OF SAR IMAGES

Several algorithms exist to form focused SAR images $s(x, r)$ from $d(x, t)$. We investigate here the constant integration angle backprojector, which is often used in UWB wide angle SAR, because motion compensation for the radar can easily be integrated into the algorithm [9].

The constant integration angle backprojector correlates $d(x, t)$ with hyperbolas over a finite aperture:

$$\begin{aligned} s(x,r) \quad = \quad & u(r)v(x) \int\int d(\hat{x}, \hat{t}) \frac{1}{\sqrt{r}} w\left(\frac{\hat{x} - x}{r}\right) * \\ & \delta\left(\hat{t} - \frac{2}{c}\sqrt{(\hat{x}-x)^2 + r^2}\right) d\hat{x}d\hat{t} \end{aligned} \tag{8}$$

The aperture is completely specified in the length and shape by its weighting function $w(\cdot)$. The two rectangular window functions $u(r)$ and $v(x)$ determine the location and size of the image patch.

Using the principle of stationary phase, Parseval's theorem and (6), the Fourier transform of $s(x, r)$ can be given in closed form

$$S(k_x, k_r) = AU(k_r)V(k_x) *_{k_r} *_{k_x} \left(G(k_x, k_r) R(k_x, k_r) I(k_x, k_r)\right) \tag{9}$$

where $G(k_x, k_r)$ is a Fourier transform derived from the reflectivity profile

$$G(k_x, k_r) = g^{x,r,t}\left(k_x, k_r, -\text{sgn}(k_r)\frac{c}{2}\sqrt{k_x^2 + k_r^2}, \frac{k_x}{k_r}\right), \tag{10}$$

$R(k_x, k_r)$ contains all the radar specific terms

$$R(k_x, k_r) = b\left(\frac{k_x}{k_r}\right) P\left(-\text{sgn}(k_r)\frac{c}{2}\sqrt{k_x^2 + k_r^2}\right), \tag{11}$$

and $I(k_x, k_r)$ includes all contributions due to the geometry of the problem and the particular image former

$$I(k_x, k_r) = |k_r|^{-1.75} \sqrt{k_x^2 + k_r^2}\, w\left(\frac{k_x}{k_r}\right) \tag{12}$$

Equation (9) is remarkable in two respects: First, the backprojected image is the result of a 2-D convolution of the (mapped) reflectivity profile $G(k_x, k_r)$ and the point-spread function $R(k_x, k_r)*$

$I(k_x, k_r)$. It provides insight into the contribution of each parameter in the radar/imaging chain to the final SAR image and allows us to remove image distortions due to the image former. Second the aspect angle and frequency dependence of the groundtruth in (1) is mapped into the image plane in the same way as the transmitted waveform $p(t)$ and the windows $w(\cdot)$ and $b(\cdot)$. Hence, angular and frequency properties of targets in $g(\cdot,\cdot,\cdot,\cdot)$ cause image features similar to the ones introduced by $p(t)$, $b(\cdot)$ and $w(\cdot)$. Consequently, many image "artifacts" contain valuable target information, which can be retrieved with properly designed post-processing algorithms.

5. SUBAPERTURE IMAGES AND DIRECTIONAL FILTERBANKS

A recent approach [3] to exploiting aspect angle target information is based on decomposing the full imaging aperture into a set of subapertures and forming a SAR image for each subaperture. Each of these images shows the imaged area for a different range of aspect angles. It has been stated [3] that this aspect angle target information can be extracted only from the raw data $d(x, t)$ and not from $s(x, r)$, because the image former integrates out all aspect angle information. However, equation (9) shows that if the support of $b(\cdot)$ is completely contained in the support of $w(\cdot)$, no information contained in the raw data is lost during imaging. Furthermore, equation (12) implies that two SAR images computed for different subapertures differ only in $w(\cdot)$. Hence, if a window $\hat{w}(\cdot)$ exists such that $w_2(\cdot) = \hat{w}(\cdot)w_1(\cdot)$, then the SAR image associated with $w_2(\cdot)$ can be computed from a SAR image formed with a subaperture specified by $w_1(\cdot)$ by filtering it with $H(k_x, k_r) = \hat{w}(\frac{k_x}{k_r})$, which has a wedge-shaped support in the frequency domain. In particular, if $w_1(\cdot)$ corresponds to the full aperture, all subaperture images can be obtained from a full aperture image by a simple shift-invariant filtering operation.

In the rest of this paper, we consider $s(n_x, n_r)$, a sampled form of $s(x, r)$ with equal sampling rates in cross-range and downrange. Images formed from subapertures have poorer cross-range resolution than the full aperture image. They can, therefore, be further decimated in cross-range by an appropriate factor without loss of information. Thus, it should be possible to decompose $s(n_x, n_r)$ into a set of subaperture images $s_\alpha(n_x, n_r)$ with non-overlapping subapertures without having to increase the overall amount of data.

Such a decomposition can be achieved with a perfect reconstructing, maximally decimated directional filterbank [4]. Figure 2a shows the geometry of the subbands. The $2\pi \times 2\pi$ frequency cell is divided into a vertical and a horizontal hourglass shaped area. Each of these two areas can be further decomposed into an arbitrary number of wedge shaped directional subbands. The frequency support of $s(n_x, n_r)$ is given as the intersection of the mapped pulse $p(\cdot)$ in (11) (the area between the two dotted circles in Fig. 2a), and the mapped window $b(\cdot)$ in (11) (the wedge shaped area between the two dotted straight lines in Fig. 2a).

We consider here only directional filterbanks with a power of 2 directional subbands in each hourglass shaped area. They can be realized either as a binary tree of two channel filterbanks [4] or in a parallel form [5]. The computation of an arbitrary subband in the parallel form is shown in 2b). The 2-D directional filters $H_\alpha(k_x, k_r)$ have to be designed such that the overall structure is invertible [4].

Using [4], the $H_\alpha(k_x, k_r)$ can be designed such that the de-

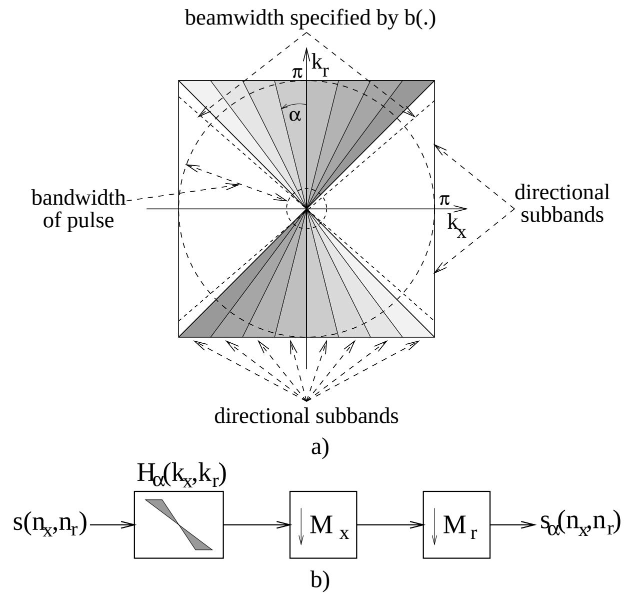

Figure 2: a) Directional subbands and frequency support of SAR data. b) One channel of directional filterbank in parallel form.

composition of the SAR image into the directional subbands is a linear, unitary transformation. Thus, the original SAR image and the collection of all subbands are two equivalent data representations. Since each directional subband corresponds to a subaperture SAR image for a different range of aspect angles, the directional subbands can be stacked to form a 3-D SAR data representation of cross-range versus downrange versus aspect angle.

6. EXAMPLE

In the following example, we use data collected with the ARL BoomSAR [9], which works in the frequency range 20-1100 MHz. The full aperture SAR images were formed with a mosaic backprojector and an integration angle of $90° \pm 4.5°$. Thus, the formed images nearly satisfy the assumptions made in our derivations. In Fig. 3a a small SAR image chip is shown. It contains a vehicle in the lower right part which is barely visible against the surrounding clutter. A directional filterbank was implemented as a binary tree. Since the applied integration angle is $90°$ no image information is contained in the horizontal hourglass shaped area. The vertical hourglass shaped area is decomposed into 8 directional subbands. The filters were realized in polyphase form, for which the necessary nonseparable filters become separable [4]. The actual one-dimensional filters are the QMF filters 32D and 48E from the appendix of [6]. The outputs of the 8 vertical subbands are shown in Fig. 3b. The aspect angle interval above each plot is given with respect to α in Fig. 2a. The vehicle is visible in the first three subbands as a directional ridge of energy with its center at coordinates (20,50).

7. APPLICATION OF DIRECTIONAL DATA DECOMPOSITION

The 3-D SAR data representation can be used to design new post-processing algorithms for SAR images. We have implemented and tested wavelet denoising [8] as a SAR postprocessing algorithm to cancel clutter and enhance target resolution. The idea of wavelet denoising is that, if a noisy signal is expanded by a unitary transformtion into a representation in which the signal is concentrated in a few coefficients, the white noise can effectively be reduced by thresholding the expansion coefficients and then applying the inverse transform. Since the features of interest in our setting are concentrated in a small number of directional subbands whereas the clutter is spread over all subbands, the same form of thresholding can be applied to the directional subbands to reduce clutter.

Our algorithm contains two steps: First we remove the point-spread function $R(k_x, k_r)I(k_x, k_r)$ from the data by inverse filtering. Then the soft-threshold mapping [8]

$$\hat{x} = \begin{cases} \operatorname{sgn}(x)(|x| - t) & \text{if } |x| \geq t \\ 0 & \text{if } |x| < t \end{cases} \tag{13}$$

is applied to each directional subband. The threshold parameter t was determined experimentally. Figure 3c shows the resynthesized, post-processed SAR image chip of Fig. 3a. The clutter has been effectively removed. Furthermore, the vehicle exhibits now a delicate continuous structure which was not visible in the original data.

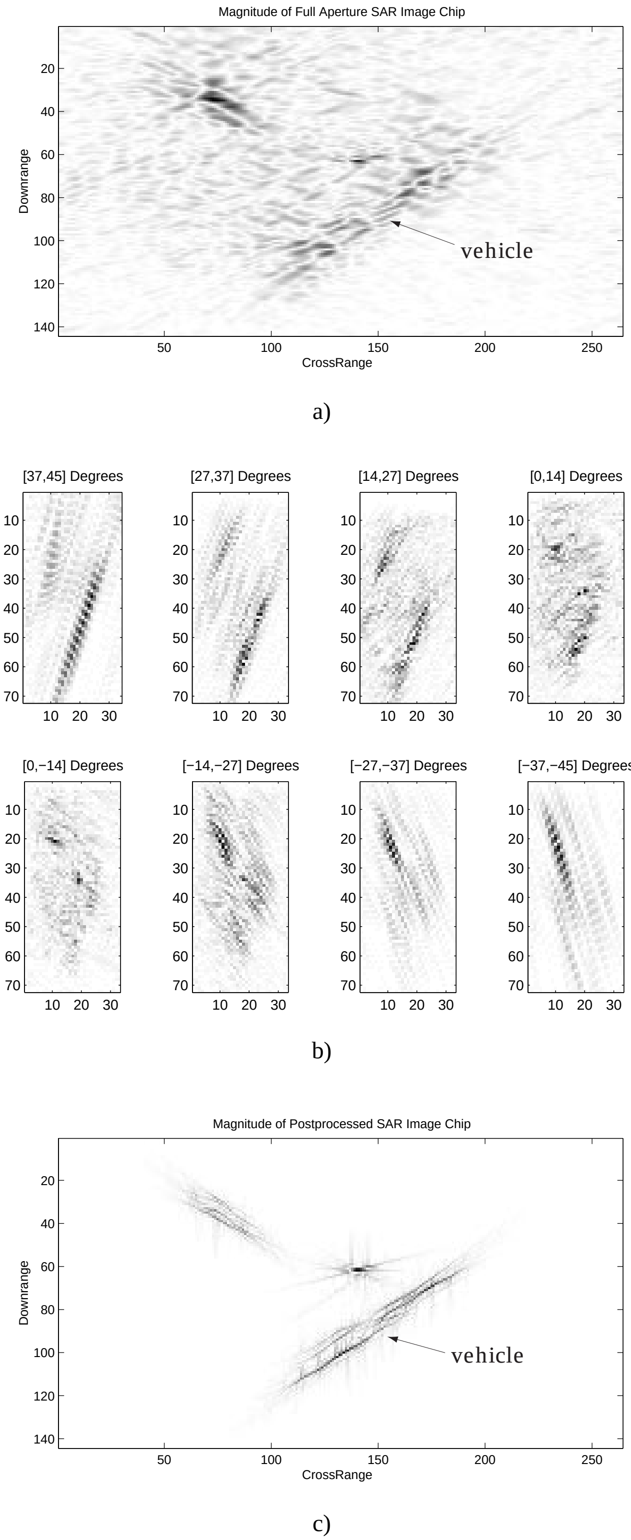

Figure 3: a) SAR image of vehicle b) vertical directional subbands of vehicle c) postprocessed SAR image chip.

8. REFERENCES

[1] M. Soumekh, “Reconnaissance with Ultra Wideband UHF Synthetic Aperture Radar”, IEEE Signal Processing Magazine, vol. 12, no.4, pp.21-40, July 1995

[2] H. Choi et al., “On the Optimality and Exactness of Wavenumber-Domain SAR Data Processing”, IEEE Trans. on Pattern Analysis and Machine Intelligence, vol. 13, no. 9, pp.891-906, 1994

[3] R. Kapoor et al., “Features for Detecting Obscured Objects in Ultra-Wideband (UWB) SAR Imagery Using A Phenomenological Approach”, Pattern Recognition, vol.29, no.11, pp.1761-1774, 1996

[4] R. H. Bamberger and M. J. T. Smith, “A Filter Bank for the Directional Decomposition of Images: Theory and Design”, IEEE Transactions on Signal Processing, vol.40, no.4, pp.882-893, April 1992

[5] R. H. Bamberger, “New Results on Two and Three Dimensional Directional Filter Banks”, Twenty-Seventh Asilomar Conference on Signals, Systems and Computers, vol. 2, pp.1286-1290, 1993

[6] R. E. Crochiere et al., “Multirate Digital Signal Processing”, Prentice-Hall, Englewood Cliffs, NJ, 1983

[7] R. D. Chaney et al., “Coherent aspect-dependent SAR image formation”, Proc. of the SPIE, vol. 2230, pp.256-274, 1994

[8] C. S. Burrus et. al., “Introduction to Wavelets and Wavelet Transforms: A Primer”, Prentice-Hall, Englewood Cliffs, NJ, 1997

[9] L. Nguyen et al. “Detection Algorithms for Ultra-Wideband Foliage Penetration Radar”, Proc. of the SPIE, vol. 3066, 1997

[10] A. I. Saichev et al., “Distributions in the Physical and Engineering Sciences: Vol. 1”, Birkhäuser, Boston, 1997